

# Accelerating Long-Tail Generation in Synchronous RLHF Training via Adaptive Tensor Parallelism

Long Zhao<sup>†,§</sup> Qinghe Wang<sup>†,§</sup> Jiaan Zhu<sup>¶</sup> Youhui Bai<sup>¶</sup> Zewen Jin<sup>¶</sup> Chaoyi Ruan<sup>‡</sup>  
Shengnan Wang<sup>\*</sup> Cheng Li<sup>¶,§</sup>

<sup>†</sup> Anhui University <sup>¶</sup> University of Science and Technology of China <sup>‡</sup> National University of Singapore <sup>\*</sup> Independent Researcher  
<sup>§</sup> Institute of Artificial Intelligence, Hefei Comprehensive National Science Center

## Abstract

Reinforcement Learning from Human Feedback (RLHF) has become a key post-training paradigm for improving model quality. However, the synchronous three-stage RLHF pipeline is often bottlenecked by the generation stage, where response-length skew causes the effective batch size to shrink rapidly during decoding, leaving GPUs underutilized while a few long responses remain unfinished. Mainstream frameworks employ a static tensor parallelism (TP) configuration that cannot adapt to changing batch characteristics, leaving substantial performance headroom unexplored.

We propose PAT, an adaptive TP method that dynamically reconfigures TP during the generation stage of each RLHF iteration. PAT introduces two key techniques. First, a predictor-guided online reconfiguration method decides both the reconfiguration point and the target TP configuration based on offline profiling, triggering reconfiguration only when the predicted latency benefit outweighs the reconfiguration overhead. Second, a lightweight online reconfiguration mechanism updates only the states and layouts affected by TP changes: it adapts unfinished decoding states through a cost-model-based choice between KV-cache migration and recomputation, performs in-place weight resharding, and reuses cached communication groups. We implement PAT on top of SGLang and integrate it with the VeRL framework. Evaluations on LLaMA3.1-8B and Qwen3-14B using DeepScaleR show that PAT reduces generation latency by up to 34.6% and end-to-end RLHF training iteration latency by up to 27.2% compared to the original VeRL setup.

## Keywords

RLHF Training, Long-Tail Generation, Tensor Parallelism, Parallelism Reconfiguration

## 1 Introduction

Reinforcement Learning from Human Feedback (RLHF) [2] has emerged as an effective post-training paradigm for aligning model outputs with human preferences and substantially improving the capabilities of large language models. Several recent prominent models, for example, DeepSeek-R1 [5], Kimi K2 [16], and OpenAI o3 [4], have adopted or explored RLHF training strategies to enhance their model quality.

The RLHF training pipeline proceeds *synchronously* through three stages in each iteration. First, the **generation stage** produces responses from the target LLM for given prompts. Second, the **preparation stage** evaluates generated responses, computing

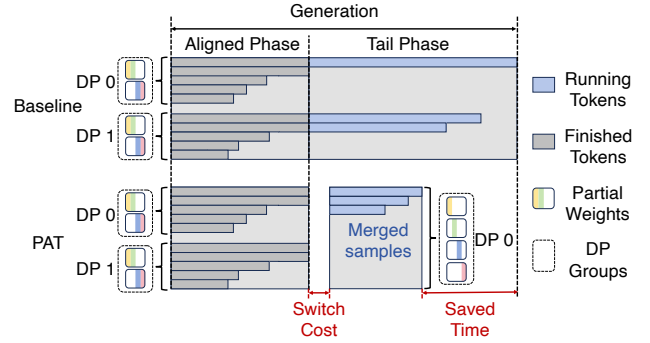


**Figure 1: Example of TP/DP reconfiguration during generation. PAT switches from (TP2, DP2) in the aligned phase to (TP4, DP1) in the tail phase.**

rewards or other auxiliary signals. Finally, the **training stage** consumes the outputs of the preparation stage, computes the training loss using the prepared signals, and updates the target LLM.

Mainstream RLHF frameworks, such as VeRL [14], prefer to collocate all three stages on the same GPU servers. Combined with synchronous execution, this reduces data movement and synchronization overhead across stages. Nevertheless, sample generation remains the primary performance bottleneck. Fig. 1 illustrates the root cause of this inefficiency. Initially, most responses have similar lengths and finish nearly simultaneously—a phase we term the **aligned phase**. Later, a small number of exceptionally long responses continue executing, entering what we call the **tail phase**. The GPU resource consumption across the two phases is highly imbalanced, leaving GPU resources severely underutilized during the tail phase. In our benchmark with a maximum response length of 16K tokens and a batch size of 128, the average per-GPU throughput drops from 13.71 TFLOPS in the aligned phase to only 0.11 TFLOPS in the tail phase. Thus, accelerating RLHF crucially depends on accelerating the tail phase caused by response-length skew.

A closer investigation reveals that these frameworks typically employ a static tensor parallelism (TP) configuration throughout the entire generation stage. While the TP degree plays a key role in determining generation performance, it remains fixed regardless of the changing batch characteristics. Under a fixed GPU budget, the large effective batch size in the aligned phase favors a smaller TP degree to achieve higher throughput. In contrast, the few remaining samples in the tail phase benefit from a larger TP degree, which

Long Zhao and Qinghe Wang equally contributed to this work.

reduces decoding latency and improves GPU utilization. This observation motivates adapting the TP degree on the fly, specifically increasing it as the effective batch size shrinks.

However, dynamically reconfiguring TP during generation is not straightforward, due to several challenges. First, TP reconfiguration incurs non-trivial overhead. Specifically, unfinished samples must be transferred or recomputed under the new parallelism layout, model weights must be resharded across the new TP group, and communication groups must be consistently updated.

Second, the benefit of reconfiguration involves a trade-off between the remaining tail workload and the reconfiguration overhead. Reconfiguring too early hurts aligned-phase throughput, as higher TP introduces extra communication and reduces data parallelism (DP) concurrency<sup>1</sup>. Reconfiguring too late leaves insufficient tail work to amortize the reconfiguration overhead. Consequently, an effective system must decide when reconfiguration is beneficial and perform it with low overhead.

To address these challenges, we propose PAT, an adaptive tensor parallelism framework that performs TP reconfiguration within the generation stage of each RLHF iteration. As shown in the lower part of Fig. 1, PAT keeps a throughput-oriented low-TP/high-DP configuration in the aligned phase, where many samples are still active. It then switches to a latency-oriented high-TP/low-DP configuration in the tail phase only when the predicted benefits outweigh the reconfiguration overhead. PAT builds on two key techniques:

First, PAT devises a predictor-guided online switching method to determine both the switching point and the target TP configuration. Relying on offline-profiled data, the predictor estimates the remaining generation latency under each candidate configuration and incorporates the one-time reconfiguration overhead into the decision. PAT triggers reconfiguration only when the predicted latency benefit on the remaining tail samples can amortize the switching cost.

Second, PAT makes reconfiguration lightweight through online runtime state and layout adaptation. Instead of reinitializing the inference engine under the target TP configuration, PAT updates only the TP-dependent states and layouts. For unfinished samples, it reconstructs decoding states through a cost-model-based choice between KV cache migration and recomputation. For model weights, it performs in-place resharding to match the target TP layout. It also reuses cached communication groups across iterations to avoid repeated group construction. Together, these mechanisms turn TP reconfiguration into a low-overhead operation, allowing tail samples to resume decoding efficiently under the new configuration.

We build PAT on SGLang [19], a widely used inference engine for RLHF generation, and integrate it with VeRL [14], one of the leading RLHF frameworks, enabling easy adoption. We evaluate PAT by training LLaMA3.1-8B [3] and Qwen3-14B [17] on DeepScaler [9]. Compared with the original VeRL setup, PAT reduces generation latency by up to 34.6%, yielding up to 27.2% lower RLHF training iteration latency.

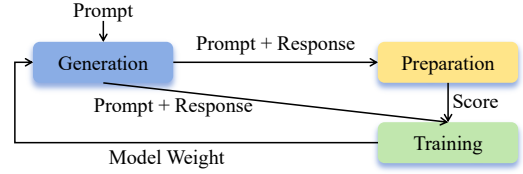


Figure 2: Typical workflow of the iterative RLHF training.

## 2 Background and Motivation

### 2.1 Workflow of RLHF

RLHF is a common approach for aligning LLMs with human preferences [5, 11]. It typically consists of supervised fine-tuning, reward model training, and reinforcement learning. This work focuses on the reinforcement learning step, including algorithms such as PPO [12], GRPO [13], and DAPO [18], where iterative generation, scoring, and model updates dominate the overall training cost. As shown in Fig. 2, this step can be further decomposed into three stages.

**Generation stage.** Given a batch of prompts, the actor model generates responses in an autoregressive manner. This stage includes prefill, which processes the input prompts and builds the KV cache, and decoding, which reuses KV states to generate subsequent tokens. Decoding is typically memory-bandwidth-bound and benefits from large effective batches [1].

**Preparation stage.** Given the generated prompt-response pairs, auxiliary models or modules such as reward and reference models compute rewards, log probabilities, or other training signals used for loss computation.

**Training stage.** The actor model performs forward and backward passes on the generated samples, computes the RL training loss using the prepared signals, and updates its parameters. The updated weights are then used by the next generation stage.

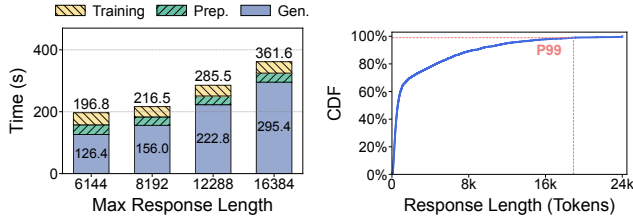
Due to these dependencies, mainstream RLHF frameworks such as VeRL [14] and RLHFuse [11] adopt colocated synchronous execution, where all stages share the same GPU pool. This deployment reduces data movement and synchronization overhead across stages.

### 2.2 Parallelism Strategies

To improve throughput and reduce per-device memory pressure, RLHF training adopts hybrid combinations of existing parallelism strategies across its three stages [10, 14]. Among these strategies, Data Parallelism (DP) replicates the model across multiple devices, with each replica processing a different subset of the batch. During training, gradients are synchronized across replicas after each iteration [8]. Tensor Parallelism (TP) splits model layers across devices, allowing computations within a single layer to be executed in parallel and reducing per-device memory usage [15]. Pipeline Parallelism (PP) partitions the model into sequential stages on different devices, passing micro-batches through the stages in a pipelined manner to overlap computation and communication [7].

The three main stages of RLHF have distinct computational demands, necessitating different parallelism strategies [14]. The preparation and training stages are typically compute-intensive

<sup>1</sup>TP is often combined with DP in practice. Although we primarily change the TP degree, doing so also results in changes to the DP configuration.



(a) End-to-end iteration latency with increasing max generation length. (b) CDF of response lengths generated by LLaMA3.1-8B on DeepScaleR.

**Figure 3: RLHF iteration breakdown and response-length distribution.**

and can benefit from hybrid parallelism, including DP, TP, and PP, depending on model size and hardware scale. In contrast, the decoding phase is primarily memory-bandwidth-bound. Its performance is optimized by maximizing batch size rather than computational throughput. Therefore, the decoding phase uses a combination of DP and TP, while favoring the largest feasible DP degree to maximize the number of concurrent decoding requests and thus improve overall throughput. PP is usually avoided during decoding because autoregressive generation produces only one token per step, so the active batch is already the main source for amortizing weight loading, KV cache access, and kernel overhead. Further micro-batching fragments the decoding workload, reduces memory-access efficiency, and may hurt overall throughput.

### 2.3 Problems in Synchronous RLHF Training

The generation stage is the primary bottleneck in synchronous RLHF training. To quantify this, we configure a tuned static parallelism strategy for each stage and follow the HybridFlow [14] setup with a batch size of 128, using LLaMA3.1-8B on the DeepScaleR [9] dataset over eight NVIDIA A40 GPUs. As shown in Fig. 3a, the generation stage consumes 64.22% to 81.7% of the total iteration time, and its share increases with the maximum response length. Across the evaluated maximum response lengths and TP/DP configurations, decoding accounts for over 90% of the generation latency.

This decoding bottleneck mainly comes from response-length skew within each batch: a small fraction of sequences can be substantially longer than the rest [21]. Once shorter sequences finish, the active batch size drops quickly, but the generation stage must still wait for the remaining long sequences to complete. These few tail sequences therefore become the critical path of generation, leaving GPUs severely underutilized [20]. For example, across the maximum response lengths evaluated in Fig. 3a, the period with only a single remaining sample accounts for 46.29%–81.58% of the generation latency. In the 16K setting with a batch size of 128, the average per-GPU achieved throughput drops from 13.71 TFLOPS in the aligned phase to only 0.11 TFLOPS near the end of generation.

This long-tail behavior is not unique to a specific dataset. Prior RLHF systems have also identified long-tail generation as a major source of stage-level inefficiency [20, 21]. Such behavior commonly appears in workloads with substantial response-length variability, including reasoning, code generation, and instruction following. To quantify this effect, we further analyze the response length

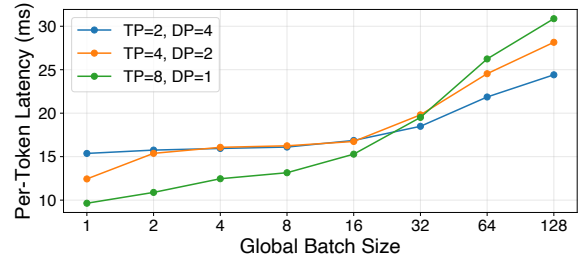


**Figure 4: Impact of TP degree and global batch size on per-token decoding latency.**

distribution of LLaMA3.1-8B on DeepScaleR. As shown in Fig. 3b, 10.85% of sequences exceed 8K tokens, and 2.18% are extreme outliers exceeding 16K tokens. With a common batch size of 128, this distribution implies that each batch contains 2.8 such extreme long-tail sequences on average, which is sufficient to create a severe tail-phase bottleneck. These observations motivate PAT to accelerate tail phase decoding in RLHF workloads with non-negligible response-length skew.

Existing systems such as StreamRL [20] mitigate long-tail bubbles by asynchronously overlapping generation with other stages. However, such approaches may introduce stale-rollout trade-offs that affect training accuracy. In contrast, PAT accelerates the tail phase within the synchronous RLHF execution flow, without changing the RLHF algorithmic semantics.

## 3 Design Rationale

### 3.1 Observation and Insight

The shrinking active batch size raises a question: should generation continue using the same TP/DP configuration in the tail phase? To answer this, we study how decoding latency changes under different TP degrees and batch sizes. Results show that the preferred TP degree is strongly batch-dependent, making a single static TP/DP configuration inefficient across the entire decoding process.

We quantify this effect using LLaMA3.1-8B on the DeepScaleR dataset. Fig. 4 reports the per-token decoding latency under different TP degrees and global batch sizes, revealing a clear batch-dependent trade-off. When the batch size is 1, increasing TP from 2 to 8 reduces the per-token latency from 15.37 ms to 9.64 ms, a 37.3% reduction. In the small-batch regime, decoding is dominated by per-token data movement from HBM to compute units. A larger TP degree shards model weights and KV states across more GPUs, reducing the data each GPU must load from HBM and increasing per-token parallelism. This reduction outweighs the extra TP communication cost. However, when the batch size increases to 128, the same TP raises the per-token latency from 24.41 ms to 30.87 ms, a 26.5% increase, because TP communication becomes dominant. These results confirm that high TP suits small-batch tail decoding, whereas a low TP better serves large-batch aligned decoding.

These observations suggest an opportunity for adaptive TP reconfiguration within a single generation stage. Specifically, a smaller TP degree can be used in the large-batch aligned phase to

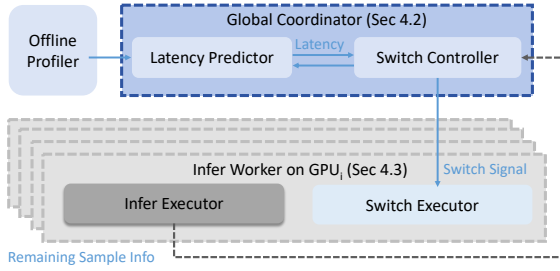


**Figure 5: Architecture of PAT with a Global Coordinator and per-GPU Inference Workers.**

avoid excessive communication overhead and maximize throughput, while a larger TP degree can be used in the small-batch tail phase to reduce the latency of the remaining sequences. Such reconfiguration also requires corresponding adjustments to DP to maintain a valid parallel configuration under a fixed total number of GPUs. Fig. 1 provides a concrete example with four GPUs. The static baseline configuration (TP=2, DP=2) is used throughout the entire process. Our solution uses (TP=2, DP=2) for the aligned phase and dynamically switches to (TP=4, DP=1) for the tail phase. This switch involves merging the remaining samples from separate DP groups into a unified batch, thereby increasing the effective batch size for the tail sequences and improving GPU utilization.

### 3.2 Challenges of TP Switching

However, adaptive TP switching within a generation stage must address the following two key questions:

#### When should the switch be triggered to maximize benefit?

The first challenge is to decide when a TP switch is beneficial. As decoding progresses, finished samples reduce the active batch size while unfinished samples accumulate longer contexts, causing the optimal TP/DP configuration to change over time. Therefore, PAT cannot rely on a fixed threshold; it must compare the predicted remaining latency under the current and candidate configurations, including the one-time reconfiguration cost, and switch only when the benefit can amortize this cost.

#### How to perform the switch efficiently with minimal extra overhead?

The second challenge is to keep reconfiguration overhead low enough to preserve the benefit of adaptive TP. Changing TP/DP requires transitioning the generation context to a new parallelism layout, including communication groups, weight partitions, and unfinished-sample states. In particular, the KV cache of unfinished samples must also be migrated or recomputed. A naive restart-based solution rebuilds these components from scratch, introducing prohibitive latency that can outweigh the benefit of switching.

## 4 System design

### 4.1 Overview

To support adaptive TP/DP reconfiguration during RLHF generation, PAT adopts a Global Coordinator and per-GPU worker architecture, as shown in Fig. 5. The Global Coordinator manages the global generation status and coordinates reconfiguration decisions across workers. It takes profiling data from the

Offline Profiler and uses the Latency Predictor and Switch Controller to decide whether to switch and which target TP/DP configuration to use, as discussed in Sec. 4.2. Following common RLHF deployments, PAT uses intra-node TP and inter-node DP. This design allows each node to reconfigure TP independently, while DP synchronization ensures the generated samples from all nodes are collected before entering the subsequent stage.

Each GPU runs an Infer Worker, which contains an Infer Executor and a Switch Executor. The Infer Executor performs normal token generation and reports the status of unfinished samples, such as active batch size and context lengths, to the Global Coordinator. When reconfiguration is triggered, the Switch Executor applies the new TP/DP configuration by handling unfinished-sample states, resharding model weights, and updating communication groups. The low-overhead switching mechanisms are described in Sec. 4.3.

### 4.2 Predictor-based Switch Timing Decision

This section first presents the overall online switching strategy, which determines both when to trigger a switch and which TP/DP configuration to select during decoding. We then describe the key components that enable this decision process, including the offline profiler and the online latency predictor.

**Online Switch Strategy.** PAT employs Algorithm 1 to make cost-based switching decisions during decoding. The algorithm is invoked repeatedly within one generation stage, so PAT can perform multiple TP/DP reconfigurations as the active batch size and context lengths change. Under a fixed GPU budget, selecting a target TP degree also determines the corresponding DP degree.

During decoding, the Infer Executor reports the runtime status of unfinished samples to the Switch Controller, including the active batch size and current sequence lengths. The controller first estimates the remaining decoding time under the current configuration (Line 4). It then enumerates each candidate TP degree. For each candidate, it computes the merged batch size after redistributing unfinished samples across DP groups (Line 7), estimates the remaining decoding time under the target configuration (Line 8), and adds the one-time switching overhead (Line 9). The remaining time is estimated using the maximum response length, which provides a conservative bound: unfinished samples may stop earlier, but they cannot exceed this length. The switching overhead includes generation-context transition costs such as unfinished-state handling, weight resharding, and communication-group updates, which are detailed in Sec. 4.3.

After evaluating all candidates, the controller selects the TP degree with the minimum total predicted cost, i.e., remaining decoding time plus switching overhead (Lines 6–14). A switch is triggered only when this cost is lower than continuing under the current configuration (Line 15), ensuring that the predicted benefit on tail samples can amortize the switching overhead. Once triggered, PAT pauses decoding, merges and redistributes unfinished samples, performs TP/DP reconfiguration, and then resumes decoding under the new configuration (Lines 23–25). Otherwise, decoding continues under the current configuration and the controller reevaluates later. **Offline Profiler.** The Offline Profiler performs a one-time automated sparse-sampling process for each  $\langle model, hardware \rangle$

**Algorithm 1** Online Switch Mechanism

---

**Require:** Current TP  $tp$ , candidate TP sizes  $tp\_list$ , remaining batch sizes for all DP groups  $rbs\_list$ , max response length  $L_{max}$ , generated length  $L_{gen}$ , running requests  $\mathcal{R}$

**Ensure:** Minimized residual decoding time

- 1:  $do\_switch \leftarrow \text{false}$
- 2:  $tp_{new} \leftarrow tp$
- 3: **while** decoding not finished **do**
- 4:  $T_{cur} \leftarrow \text{est\_rem\_time}(tp, rbs\_list, L_{max}, L_{gen})$
- 5:  $T_{best} \leftarrow \infty$
- 6: **for** each  $tp' \in tp\_list$  **do**
- 7:  $bs' \leftarrow \text{compute\_merged\_bs}(rbs\_list, tp')$
- 8:  $T_{rem} \leftarrow \text{est\_rem\_time}(tp', bs', L_{max}, L_{gen})$
- 9:  $T_{total} \leftarrow T_{rem} + T_{switch}(tp, tp')$
- 10: **if**  $T_{total} < T_{best}$  **then**
- 11:  $T_{best} \leftarrow T_{total}$
- 12:  $tp_{new} \leftarrow tp'$
- 13: **end if**
- 14: **end for**
- 15: **if**  $tp_{new} \neq tp$  **and**  $T_{cur} > T_{best}$  **then**
- 16:  $do\_switch \leftarrow \text{true}$
- 17: // Exit decoding to perform TP switch
- 18: **break**
- 19: **end if**
- 20: // Continue decoding
- 21: **end while**
- 22: **if**  $do\_switch$  **then**
- 23:  $\text{merge\_and\_redistribute}(\mathcal{R})$
- 24:  $\text{switch\_parallel}(tp, tp_{new})$
- 25: // Resume decoding
- 26: **end if**

---

deployment across TP degrees, batch sizes, and context lengths. Since tensor parallelism is typically confined to a single node and practical TP degrees are usually powers of two, we profile four TP configurations:  $TP \in \{1, 2, 4, 8\}$ .

To balance profiling efficiency and prediction accuracy, we sample only the feasible workload region. In our A40 experiments, we profile 10 representative batch sizes  $B \in [1, 256]$  and context lengths  $L \in [8, 128K]$ . To avoid unrealistic long-context/high-batch combinations, we retain a profiling point  $(B, L)$  only if  $B \cdot L \leq T_{cap}$ , where  $T_{cap}$  is the deployment-level active-token budget determined by the runtime KV cache capacity. For LLaMA3.1-8B on eight A40 GPUs, we set  $T_{cap} = 2^{20}$  tokens, corresponding to a conservative budget of 128K tokens per GPU. We further increase the profiling density for short contexts, e.g.,  $L < 512$ , where decoding latency shows more pronounced nonlinear behavior.

For each profiled batch size, we measure decoding latency using dummy batches to obtain controlled profiling points with fixed shapes. Real dataset samples have irregular and uneven length distributions, making it difficult to cover the desired  $(B, L)$  grid systematically. Therefore, for a target batch size  $B$  and context length  $L$ , we randomly generate token IDs of length  $L$  for each sequence and inject them as prefixes. During prefix construction, we record the corresponding prefill latency, which is later used to estimate the recomputation cost in Sec. 4.3. We then run the

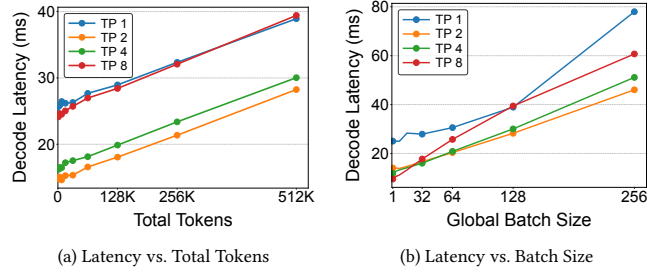


**Figure 6: Characterization of decoding latency on an H100 GPU cluster under varying total tokens and batch sizes. (a) shows the near-linear scaling with respect to the aggregate token count  $T = B \times L$  for a fixed batch size  $B = 128$ . (b) shows shape-dependent nonlinear variations as the batch size  $B$  changes for a fixed context length  $L = 4096$ .**

following 60 decoding steps and use their average latency as the per-token decoding latency at that context length.

This profiling avoids generating tokens from scratch up to each target length, reducing each measurement to only one prefix construction followed by a short decoding window. As a result, the total profiling time is reduced to approximately 10 minutes.

**Online Latency Predictor.** This module estimates two costs for the Switch Controller: the per-step decoding latency for a runtime workload and the one-time reconfiguration cost between TP/DP configurations.

As shown in Fig. 6, decoding latency is mainly determined by the active batch size  $B$  and the aggregate context token count  $T = \sum_{i=1}^B (L_i^{prompt} + L_i^{gen})$ . Although latency generally increases with  $T$ , it also varies nonlinearly across batch sizes due to kernel tiling, hardware alignment, and backend-specific optimizations. To capture these effects efficiently, PAT builds a piecewise linear predictor from sparse profiling data. At runtime, for a workload  $(B, T)$  under a candidate TP degree, the predictor queries the fitted latency curves of the two nearest profiled batch sizes and interpolates along the batch dimension to obtain the per-step latency  $\ell(B, T; TP)$ .

The predictor also estimates the one-time reconfiguration cost. This cost includes data-movement overheads, such as model-weight resharding and unfinished-sample state handling, and control overheads, such as CUDA Graph recapturing, memory deallocation, and garbage collection. For unfinished-sample states, PAT uses the lower estimated cost between KV cache migration and recomputation, as detailed in Sec. 4.3. These estimates allow PAT to trigger TP/DP reconfiguration only when the expected tail-decoding benefit can amortize the transition cost.

Overall, the predictor is tied to the deployment setting rather than a specific dataset. Its inputs are the model, hardware/backend, TP/DP configuration, active batch size, and aggregate context tokens. Different datasets mainly affect the runtime values of  $B$  and  $T$ , so the same profiled predictor can be reused across datasets under the same deployment.

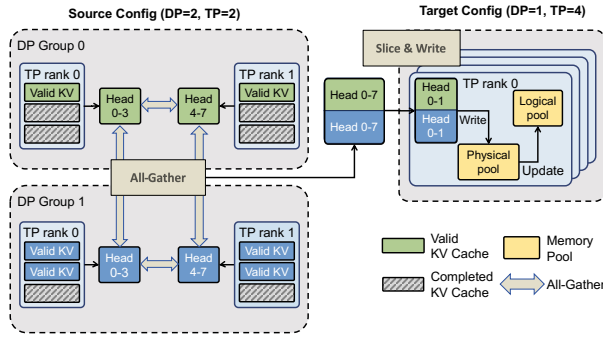


Figure 7: Workflow of KV cache migration.

### 4.3 Low-overhead Parallelism Switching

To mitigate the overhead of TP switching, PAT circumvents restarting the inference engine by employing a set of reuse mechanisms with optimization trade-offs.

**State handling for unfinished samples.** During TP reconfiguration, PAT restores unfinished samples using either KV cache migration or recomputation. Migration transfers valid KV states to the target TP/DP configuration, avoiding extra prefill computation but introducing communication overhead. Recomputation transfers only token sequences and rebuilds KV states through an additional prefill pass. The Latency Predictor estimates both costs for each candidate configuration and uses  $\min(T_{\text{move}}, T_{\text{recomp}})$  as the predicted state-handling cost.

For KV cache migration, PAT estimates  $T_{\text{move}}$  from the amount of valid KV data on the communication critical path. As shown in Fig. 7, PAT redistributes KV states using a layer-wise All-Gather and Slice procedure. GPUs first gather the valid KV shards of unfinished samples within the target TP group, and each target TP rank then slices out its required head partition. This is necessary because source KV shards are organized according to the old DP/TP layout; after DP groups are merged and TP degree is changed, a target rank may not hold the KV heads it needs locally. All-Gather and Slice reconstructs the logical KV states under the new TP group while preserving the engine’s canonical rank-to-shard mapping.

Let  $B$  be the number of unfinished samples,  $L_i$  the context length of the  $i$ -th unfinished sample,  $M$  the number of Transformer layers,  $H$  the hidden dimension,  $s$  the bytes per element, and  $\text{TP}_{\text{src}}$  the source TP degree. Since KV states are sharded across source TP ranks, the per-rank KV send volume is approximated as

$$S_{\text{kv}}^{\text{rank}} = \sum_{i=1}^B 2 \cdot M \cdot L_i \cdot \frac{H}{\text{TP}_{\text{src}}} \cdot s, \quad (1)$$

where the factor 2 accounts for key and value tensors. Given the measured one-way per-rank bandwidth  $B_{\text{net}}^{\text{uni}}$  under the same migration pattern, PAT estimates

$$T_{\text{move}} = \frac{S_{\text{kv}}^{\text{rank}}}{B_{\text{net}}^{\text{uni}}}. \quad (2)$$

Here,  $B_{\text{net}}^{\text{uni}}$  denotes one-way per-rank bandwidth rather than bidirectional aggregate PCIe/NVLink bandwidth.

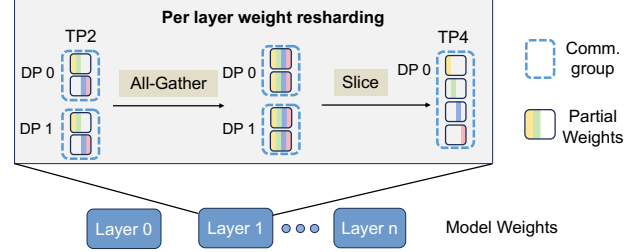


Figure 8: Reload-free layer-wise weight resharding.

For recomputation, PAT reruns batched prefill for all unfinished samples under the target TP/DP configuration. Because unfinished samples may have different context lengths while the Offline Profiler records the latency of fixed-length batches, we approximate the variable-length batch with an equivalent fixed-length batch using the root-mean-square (RMS) context length. Let  $\tilde{L}_i$  be the full context length of the  $i$ -th unfinished sample:

$$L_{\text{RMS}} = \sqrt{\frac{1}{B} \sum_{i=1}^B \tilde{L}_i^2}. \quad (3)$$

This preserves the dominant quadratic attention cost in prefill, i.e.,  $BL_{\text{RMS}}^2 = \sum_{i=1}^B \tilde{L}_i^2$ . The recomputation time is estimated as

$$T_{\text{recomp}} = T_{\text{prefill}}^{\text{prof}}(B, L_{\text{RMS}}; \text{TP}_{\text{target}}), \quad (4)$$

where  $T_{\text{prefill}}^{\text{prof}}(B, L; \text{TP})$  denotes the profiled prefill latency for batch size  $B$  and context length  $L$  under TP configuration TP.

**Efficient weight resharding.** Varying the TP degree leads to different sharding granularities of model weights across GPUs. A naïve approach to handle this transition is to reload weights from the training engine into the inference engine. However, format mismatches introduce substantial overhead from loading, conversion, and resharding, which is further exacerbated by CPU-to-GPU data transfers under parameter offloading. We observe that during the same generation stage, the weight contents remain unchanged, and only their partitioning shapes change with the TP degree.

Based on this observation, PAT employs a reload-free, layer-wise resharding strategy, as illustrated in Fig. 8. To transition between TP/DP configurations efficiently, we implement a communication-based redistribution mechanism using a sequence of layer-wise All-Gather and Slice operations. Instead of a monolithic transfer, we process weights layer-by-layer to strictly bound the peak memory usage, ensuring that the resharding process does not trigger out-of-memory (OOM) errors even under high memory pressure.

Although some local shards may already match the target layout, relying on such reuse would require changing the engine’s canonical rank-to-shard mapping. Since weight layout, TP collectives, and CUDA Graphs all assume a fixed order between TP ranks and tensor partitions, PAT explicitly reshards weights to preserve SGLang’s rank semantics.

**Reuse of communication groups.** Updating the TP degree requires reconfiguring communication groups to ensure that distributed model weight shards can correctly execute collective operations. To avoid the overhead of repetitive initialization, PAT

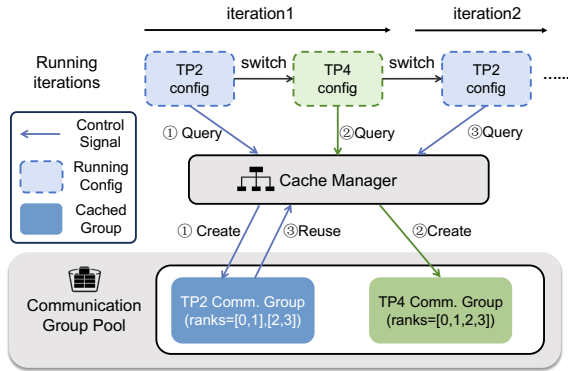


**Figure 9: Lifecycle of communication group reuse. The Cache Manager avoids redundant initialization by caching instantiated process groups across iterations.**

implements a Cache Manager that maintains a Communication Group Pool in each worker process.

As illustrated in Fig. 9, the lifecycle of a communication group involves a *lazy initialization and persistent caching* strategy. When a TP/DP configuration is requested for the first time, the Cache Manager creates the corresponding process groups and stores their handles in the pool. In subsequent iterations, the required communication groups are directly retrieved from the pool via cache hits. Consequently, over the full lifecycle of RLHF training, only the first appearance of a specific TP/DP configuration incurs group initialization cost. Given that tensor parallelism is typically restricted to a single node, the number of candidate configurations is strictly limited (e.g.,  $TP \in \{1, 2, 4, 8\}$ ). Empirical measurements on our A40 single-node experiments show that the memory footprint for maintaining these idle communication handles is negligible (contributing only an additional 2% of GPU memory usage).

**Correctness-preserving reconfiguration.** The above reconfiguration preserves the original RLHF semantics. PAT does not change the rollout policy, reward computation, loss function, or model update rule; it only changes tensor placement across GPUs. In the migration path, KV cache handling and weight resharding use tensor copy, All-Gather, Slice, and metadata updates, which only reorder existing shards without arithmetic reduction, accumulation, quantization, or precision conversion. Thus, they introduce no additional floating-point error. In the recomputation path, PAT rebuilds KV states by running the same prefill computation with the same token sequence and model weights, matching the numerical behavior of the original backend. Overall, PAT preserves synchronous RLHF semantics without introducing extra numerical approximation beyond standard GPU execution.

#### 4.4 Implementation Details

PAT is built on top of VeRL [14] and SGLang [19]. VeRL orchestrates the RLHF workflow, while SGLang serves as the generation engine where runtime TP/DP reconfiguration is performed.

**Adaptation to RL framework.** On the VeRL side, we add 895 lines of code to adapt the generation orchestration. The original

VeRL generation stage implements DP by launching multiple independent inference engines, which works for static execution but prevents coordinated TP/DP reconfiguration due to isolated runtime states and process management. PAT therefore replaces the multi-engine generation mode with a unified single-engine mode, allowing all inference workers to be managed under one SGLang engine instance. This change is an enabling mechanism for coordinated reconfiguration rather than an independent optimization: the generation kernels, batching policy, and static TP/DP execution remain unchanged when switching is disabled.

**Adaptation to inference engine.** On the SGLang side, we add about 2,650 lines of code to support online TP/DP switching, including runtime reconfiguration, CUDA Graph management, and reuse of configuration-independent inference modules.

A practical challenge is that inference engines commonly capture CUDA Graphs for different batch sizes to accelerate decoding. When PAT switches TP/DP configurations, the shapes of input tensors and weight shards change, so CUDA Graphs captured under the original configuration become invalid and cannot be directly reused. Recapturing graphs for all possible batch sizes would introduce noticeable overhead from warm-up, graph capture, and runtime variable initialization. To reduce this overhead, PAT only captures CUDA Graphs for small batch sizes that may appear after switching in the tail phase, while avoiding unnecessary graph construction for large aligned-phase batches.

In addition, we avoid reinitializing runtime modules whose states are independent of the TP/DP configuration, such as the tokenizer and grammar backend. These modules are reused across reconfigurations, reducing switching overhead without affecting the generation kernels, batching policy, or decoding semantics.

## 5 Evaluation

### 5.1 Experimental Setup

**Testbed.** To comprehensively evaluate the performance and adaptability of PAT, we conduct experiments on two types of GPU clusters. First, we deploy PAT on a cluster of two nodes (16 GPUs total), with each node equipped with 8 NVIDIA A40 48GB GPUs connected via PCIe  $4.0 \times 16$ , while inter-node connectivity is provided by 100Gbps InfiniBand. Additionally, we evaluate performance on a single high-performance server equipped with 8 NVIDIA H100 80GB SXM GPUs, connected via NVLink with a bidirectional bandwidth of 900 GB/s. Our experiments use the following software versions: CUDA 12.6, PyTorch 2.7.1, VeRL 0.4.1, and SGLang 0.4.8.

**Model and dataset.** We adopt the widely used GRPO algorithm [13] for RLHF. We use LLaMA3.1-8B [3] and Qwen3-14B [17] as actor models. For the training data, we employ the DeepScaleR [9], which is a logic-intensive dataset designed to enhance reasoning capabilities through RL. This dataset provides a representative stress test for PAT, as its response length distribution exposes the tail-phase bottleneck targeted by our design.

**Baseline and metric.** We compare PAT against VeRL, a state-of-the-art colocated RLHF training framework. To ensure a fair comparison, for each model, hardware setting, and maximum response length, we tune the static TP/DP configuration of VeRL among feasible settings and report the best-performing baseline. Our primary evaluation metric is throughput, defined as the ratio

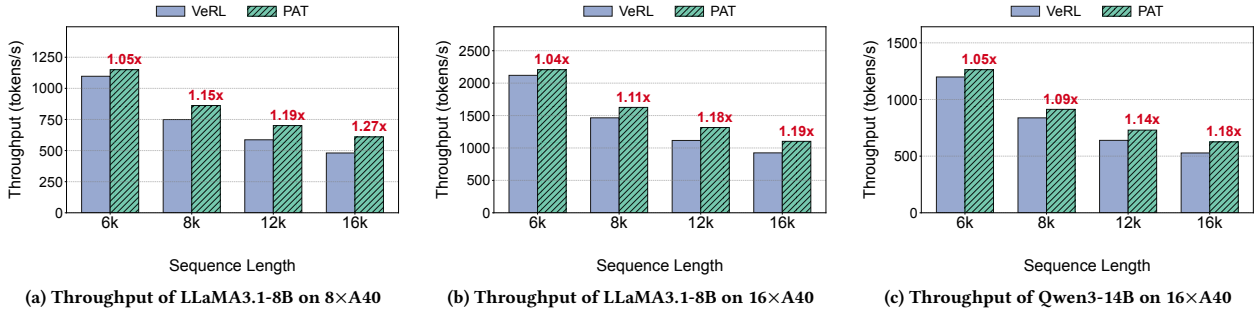


**Figure 10: End-to-end throughput comparison between VeRL and PAT on the A40 cluster. (a) and (b) compare the end-to-end throughput under increasing sequence lengths for LLaMA3.1-8B on single-node and dual-node, respectively. (c) compares the end-to-end throughput under increasing sequence lengths for Qwen3-14B on dual-node.**

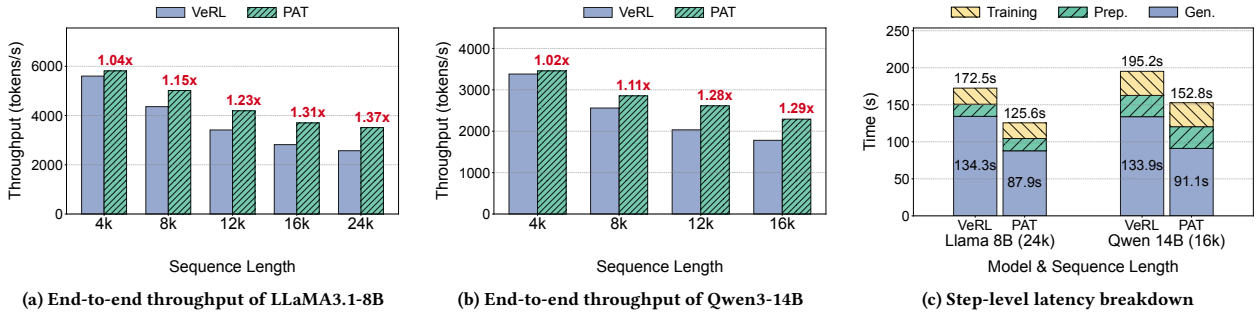


**Figure 11: Comprehensive performance evaluation on the H100 server. (a) and (b) compare the end-to-end throughput under increasing sequence lengths for LLaMA3.1-8B and Qwen3-14B models. (c) illustrates the detailed time breakdown of training steps for LLaMA3.1-8B (24k) and Qwen3-14B (16k).**

of the total number of tokens generated in a single RLHF step to the duration of that step. For each maximum response length, we report the average latency over five stable RLHF steps in which at least one generated sample reaches the specified maximum length.

## 5.2 End-to-End Throughput

**Results on A40 Cluster.** We conduct end-to-end throughput evaluations on an A40 cluster to verify the effectiveness of PAT, utilizing LLaMA3.1-8B and Qwen3-14B across both single-node (8x A40) and dual-node (16x A40) configurations with varying sequence lengths.

On the single 8x A40 server with LLaMA3.1-8B (Fig. 10a), PAT achieves speedups ranging from 1.05x to 1.27x. A notable trend is that the acceleration becomes increasingly pronounced as the sequence length increases (from 6k to 16k). This advantage stems from PAT’s adaptive TP strategy. As the context length grows, the tail phase becomes more severe and occupies a larger proportion of the total runtime, thereby maximizing the benefits of our targeted optimization under preferred parallel configurations. This confirms the effectiveness of PAT in mitigating severe tail bottlenecks.

When scaling the same LLaMA3.1-8B setup to the dual-node configuration (16x A40, Fig. 10b), PAT still delivers consistent improvements, achieving up to 1.19x speedup. Although the speedup

is slightly limited by inter-node communication for DP synchronization during the training stage of each RLHF iteration, the consistent gains validate the scalability of PAT in distributed settings.

To verify the impact of different model architectures, we replace the model with the larger Qwen3-14B in the dual-node environment (Fig. 10c). Here, PAT delivers speedups ranging from 1.05x to 1.18x. We observe that these gains are relatively lower than those of LLaMA3.1-8B under the same dual-node setting. This disparity occurs because Qwen3-14B’s larger communication volume increases the fraction of time spent on communication under the limited PCIe bandwidth, making it the dominant bottleneck. Nevertheless, consistent gains across model architectures confirm that PAT remains robust and effective even under hardware bandwidth constraints.

**Results on H100 Server.** To further validate the effectiveness of PAT on high-end GPU platforms, we conduct an end-to-end throughput evaluation on a single 8-GPU H100 server. As shown in Fig. 11a and Fig. 11b, PAT outperforms VeRL on both models. The H100 results mirror the trend observed on the A40 cluster: the relative speedup of PAT increases with the maximum response length. For LLaMA3.1-8B, PAT achieves 3510.9 tokens/s at a maximum response length of 24K, corresponding to a 1.37x speedup over VeRL (2570.6 tokens/s). For Qwen3-14B, PAT achieves 2292.6 tokens/s at 16K, yielding a 1.29x speedup over VeRL (1780.0 tokens/s).

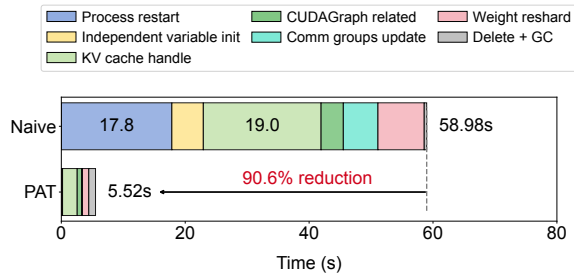


**Figure 12: Switching latency breakdown comparison between Naive and PAT on the A40 cluster (LLaMA3.1-8B, triggered at 12k context with 9 samples remaining).**

Notably, PAT achieves larger speedups on the H100 server than on the A40 cluster. NVLink’s higher communication bandwidth reduces both the overhead of larger TP degrees and the cost of online reconfiguration. As a result, in the tail phase where only a few long responses remain active, higher TP more effectively reduces per-token latency and more easily amortizes the switching cost. This shows that PAT can better exploit high-bandwidth GPU platforms for long-tail RLHF generation.

### 5.3 Step-level Breakdown

To understand the source of the end-to-end speedup, we analyze the step-level latency breakdown of representative H100 runs. As shown in Fig. 11c, PAT mainly reduces the generation time, which is the stage targeted by adaptive TP reconfiguration.

For LLaMA3.1-8B with a maximum response length of 24K, PAT reduces generation time from 134.3 s to 87.9 s, achieving a 34.6% reduction. This leads to a 1.37 $\times$  end-to-end speedup, with the overall step latency decreasing from 172.5 s to 125.6 s. For Qwen3-14B at 16K, PAT similarly reduces generation time from 133.9 s to 91.1 s, corresponding to a 32.0% reduction. Meanwhile, the preparation and training stages vary by less than 1.5%, indicating that PAT improves RLHF efficiency by directly reducing the long-tail generation bottleneck without shifting overhead to other stages.

### 5.4 Switching Overhead

**Analysis of switching time.** We evaluate the switching overhead of PAT against a naive restart-based approach. We use the A40 cluster with a TP2-to-TP8 switch at a 12k context length and 9 remaining samples as a representative high-overhead case, due to PCIe bandwidth limits and large KV-transfer volume. As shown in Fig. 12, the naive approach takes 58.98 s due to process restarts, memory re-initialization, full KV recomputation, and weight reloading. In contrast, PAT reduces the switching cost to 5.52 s, achieving a 90.6% reduction. This overhead accounts for only 1.23% of the 447 s end-to-end runtime. Without these optimizations, the runtime would increase by 53.46 s to 500.46 s, offsetting much of the tail-phase acceleration from larger TP.

The reduction in switching overhead mainly comes from optimized data movement and runtime-state reuse. First, reload-free layer-wise redistribution reduces weight resharding from 7.47 s

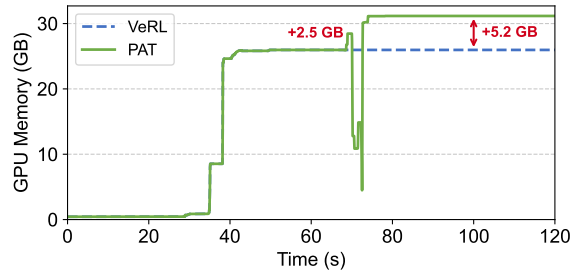


**Figure 13: Memory footprint during the switching phase for LLaMA3.1-8B on the DeepScaleR dataset using 8 $\times$ A40 single-node configuration.**

to 1.03 s. Second, migrating only valid KV states reduces KV handling from 19.01 s to 2.36 s compared with full prefill. Third, CUDA Graph recapturing is reduced from 3.59 s to 0.73 s by only targeting the small batch sizes that may appear after switching, while communication groups and other independent initialization tasks are reused when possible. We also observe that the switching overhead remains nearly unchanged in multi-node settings under the same 12K-token context length at the switching point, because TP switching is confined to each node, enabling parallel switching across independent DP groups. Thus, the overall latency is determined by the per-node switching time rather than the number of nodes.

**Analysis of extra memory overhead.** We further analyze the memory overhead during switching. As shown in Fig. 13, a naive full-state migration would require moving the entire 14 GB KV cache and may trigger OOM. In contrast, PAT increases peak memory usage by only 2.5 GB during switching, because it extracts only valid KV payloads and redistributes them layer by layer. The 5.2 GB increase in steady-state memory after switching comes from reallocating a larger KV cache pool required by the new TP configuration, rather than from intrinsic overhead introduced by PAT.

### 5.5 Predictor Effectiveness

To validate the reliability of our reconfiguration decisions, we evaluate whether the predictor built from dummy-batch profiling can accurately estimate performance on real dataset-derived workloads. Although the Offline Profiler collects latency profiles using synthetic fixed-shape batches rather than dataset samples, we compare the predicted throughput against ground-truth measurements on real decoding trajectories from the DeepScaleR [9] dataset under TP degrees of 2 and 8.

As illustrated in Fig. 14, the predictor closely matches the real throughput trajectories as the number of remaining samples decreases during batch draining. Quantitatively, it achieves low average prediction errors of 4.04% for TP=2, DP=4 and 3.07% for TP=8, DP=1 on the DeepScaleR dataset. Notably, as shown in Fig. 14b, the TP8 trajectory exhibits a local non-monotonic fluctuation caused by shape-dependent backend behavior. Despite this irregularity, the predictor captures both the overall decreasing trend and the local throughput jump. These results demonstrate that our profiling method is dataset-independent and can still provide high-accuracy predictions for real decoding workloads.

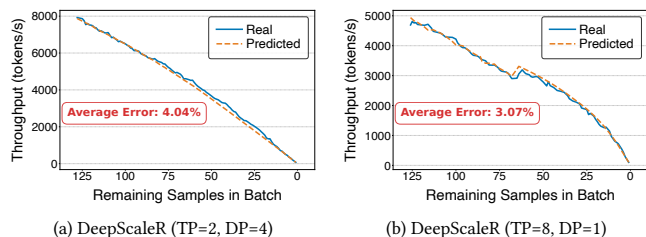


**Figure 14: Evaluation of throughput prediction accuracy across different TP degrees. The plots compare the real and predicted throughput on the DeepScaleR dataset.**

## 5.6 Discussion

Long-tail generation is common in synchronous RLHF workloads rather than a corner case. Prior work has observed pronounced response-length skew in open-ended dialogue traces such as LMSYS-Chat-1M, as well as in reasoning-oriented math/code RL workloads [20, 21]. PAT targets this common setting by adapting the TP/DP configuration as the active batch size shrinks during decoding. For workloads with short or nearly uniform responses, the tail phase is less pronounced, so PAT may provide smaller gains; in such cases, the predictor avoids switching unless the estimated benefit exceeds the reconfiguration cost.

## 6 Related Work

Several systems have been proposed to improve the efficiency and usability of RLHF training. OpenRLHF [6] provides an easy-to-adopt open-source platform, but typically partitions cluster resources across different RLHF components, which can lead to low utilization during sequential stage execution. VeRL [14] improves resource sharing through a colocated architecture and flexible RLHF data flows, yet its generation stage still relies on static parallelism and remains vulnerable to long-tail decoding. StreamRL [20] mitigates stage-level bubbles by enabling asynchronous execution between generation and training, but such benefits are limited in strictly synchronous RLHF settings and may introduce stale-rollout tradeoffs. PAT instead focuses on improving generation efficiency within the synchronous execution model by adaptively reconfiguring the TP degree during a single generation stage.

Recent systems have explored different ways to mitigate long-tail generation in RLHF. RLHFuse [21] mitigates long-tail stalls through inter-stage overlap, hiding part of the tail latency with preparation-stage execution. However, this benefit relies on sufficient preparation work and can be limited when the preparation stage is short, such as in GRPO without a critic, settings without a reward model, or iterations dominated by long-tail generation. Moreover, inter-stage overlap does not directly reduce the decoding latency of the tail samples themselves. Kimi K2 [16] adopts partial rollout, which pauses unfinished long-tail trajectories and resumes them in later RL iterations to prevent them from blocking the current rollout process. However, this breaks synchronous RLHF semantics because different parts of the same trajectory may be generated by different actor checkpoints, introducing off-policy or mixed-policy rollouts and potentially posing risks to training stability or final accuracy. In contrast, PAT preserves synchronous

RLHF semantics and directly accelerates tail-phase decoding within a single generation stage through adaptive TP reconfiguration.

## 7 Conclusion

We present PAT, an adaptive TP reconfiguration framework for accelerating long-tail generation in synchronous RLHF training. PAT dynamically adjusts the TP/DP configuration within each generation stage to better match the aligned and tail phases. Implemented on SGLang and integrated with VeRL, PAT reduces generation latency by up to 34.6% and training iteration time by up to 27.2%.

## References

- [1] Amey Agrawal, Nitin Kedia, Ashish Panwar, Jayashree Mohan, Nipun Kwatra, Bhargav Gulavani, Alexey Tumanov, and Ramachandran Ramjee. 2024. Taming Throughput-Latency tradeoff in LLM inference with Sarathi-Serve. In *18th USENIX symposium on operating systems design and implementation (OSDI 24)*, 117–134.
- [2] Yuntao Bai, Andy Jones, Kamal Ndousse, Amanda Askell, Anna Chen, Nova DasSarma, Dawn Drain, Stanislav Fort, Deep Ganguli, Tom Henighan, et al. 2022. Training a helpful and harmless assistant with reinforcement learning from human feedback. *arXiv preprint arXiv:2204.05862* (2022).
- [3] Abhimanyu Dubey, Abhinav Jauhri, Abhinav Pandey, Abhishek Kadian, Ahmad Al-Dahle, Aiesha Letman, Akhil Mathur, Alan Schelten, Amy Yang, Angela Fan, et al. 2024. The llama 3 herd of models. *arXiv e-prints* (2024), arXiv–2407.
- [4] Ahmed El-Kishky, Alexander Wei, Andre Saraiva, Borys Minaiev, Daniel Selsam, David Dohan, Francis Song, Hunter Lightman, Ignasi Clavera, Jakub Pachocki, et al. 2025. Competitive programming with large reasoning models. *arXiv preprint arXiv:2502.06807* (2025).
- [5] Daya Guo, Dejian Yang, Haowei Zhang, Junxiao Song, Ruoyu Zhang, Runxin Xu, Qihao Zhu, Shirong Ma, Peiyi Wang, Xiao Bi, et al. 2025. Deepseek-r1: Incentivizing reasoning capability in llms via reinforcement learning. *arXiv preprint arXiv:2501.12948* (2025).
- [6] Jian Hu, Xibin Wu, Wei Shen, Jason Klein Liu, Zilin Zhu, Weixun Wang, Songlin Jiang, Haoran Wang, Hao Chen, Bin Chen, et al. 2024. Openrlhf: An easy-to-use, scalable and high-performance rlhf framework. *arXiv preprint arXiv:2405.11143* (2024).
- [7] Yanping Huang, Youlong Cheng, Ankur Bapna, Orhan Firat, Dehao Chen, Mia Chen, HyoukJoong Lee, Jiquan Ngiam, Quoc V Le, Yonghui Wu, et al. 2019. Gpipe: Efficient training of giant neural networks using pipeline parallelism. *Advances in neural information processing systems* 32 (2019).
- [8] Shen Li, Yanli Zhao, Rohan Varma, Omkar Salpekar, Pieter Noordhuis, Teng Li, Adam Paszke, Jeff Smith, Brian Vaughan, Pritam Damania, et al. 2020. Pytorch distributed: Experiences on accelerating data parallel training. *arXiv preprint arXiv:2006.15704* (2020).
- [9] Michael Luo, Sijun Tan, Justin Wong, Xiaoxiang Shi, William Y Tang, Manan Rongta, Colin Cai, Jeffrey Luo, Tianjun Zhang, Li Erran Li, et al. 2025. Deepscaler: Surpassing o1-preview with a 1.5 b model by scaling rl. *Notion Blog* (2025).
- [10] Zhiyu Mei, Wei Fu, Kaiwei Li, Guangju Wang, Huanchen Zhang, and Yi Wu. 2024. Realhf: Optimized rlhf training for large language models through parameter reallocation. *arXiv e-prints* (2024), arXiv–2406.
- [11] Long Ouyang, Jeffrey Wu, Xu Jiang, Diogo Almeida, Carroll Wainwright, Pamela Mishkin, Chong Zhang, Sandhini Agarwal, Katarina Slama, Alex Ray, et al. 2022. Training language models to follow instructions with human feedback. *Advances in neural information processing systems* 35 (2022), 27730–27744.
- [12] John Schulman, Filip Wolski, Prafulla Dhariwal, Alec Radford, and Oleg Klimov. 2017. Proximal policy optimization algorithms. *arXiv preprint arXiv:1707.06347* (2017).
- [13] Zhihong Shao, Peiyi Wang, Qihao Zhu, Runxin Xu, Junxiao Song, Xiao Bi, Haowei Zhang, Mingchuan Zhang, YK Li, Yang Wu, et al. 2024. Deepseekmath: Pushing the limits of mathematical reasoning in open language models. *arXiv preprint arXiv:2402.03300* (2024).
- [14] Guangming Sheng, Chi Zhang, Zilingfeng Ye, Xibin Wu, Wang Zhang, Ru Zhang, Yanghua Peng, Haibin Lin, and Chuan Wu. 2025. Hybridflow: A flexible and efficient rlhf framework. In *Proceedings of the Twentieth European Conference on Computer Systems*, 1279–1297.
- [15] Mohammad Shoeybi, Mostofa Patwary, Raul Puri, Patrick LeGresley, Jared Casper, and Bryan Catanzaro. 2019. Megatron-lm: Training multi-billion parameter language models using model parallelism. *arXiv preprint arXiv:1909.08053* (2019).
- [16] Kimi Team, Yifan Bai, Yiping Bao, Guanduo Chen, Jiahao Chen, Ningxin Chen, Ruijue Chen, Yanru Chen, Yunkun Chen, Yutian Chen, et al. 2025. Kimi k2: Open agentic intelligence. *arXiv preprint arXiv:2507.20534* (2025).
- [17] An Yang, Anfeng Li, Baosong Yang, Beichen Zhang, Binyuan Hui, Bo Zheng, Bowen Yu, Chang Gao, Chengen Huang, Chenxu Lv, et al. 2025. Qwen3 technical

- report. *arXiv preprint arXiv:2505.09388* (2025).
- [18] Qiyang Yu, Zheng Zhang, Ruofei Zhu, Yufeng Yuan, Xiaochen Zuo, Yu Yue, Weinan Dai, Tiantian Fan, Gaohong Liu, Lingjun Liu, et al. 2025. Dapo: An open-source llm reinforcement learning system at scale. *arXiv preprint arXiv:2503.14476* (2025).
- [19] Lianmin Zheng, Liangsheng Yin, Zhiqiang Xie, Chuyue Livia Sun, Jeff Huang, Cody Hao Yu, Shiyi Cao, Christos Kozyrakis, Ion Stoica, Joseph E Gonzalez, et al. 2024. Sglang: Efficient execution of structured language model programs. *Advances in neural information processing systems* 37 (2024), 62557–62583.
- [20] Yinmin Zhong, Zili Zhang, Xiaoni Song, Hanpeng Hu, Chao Jin, Bingyang Wu, Nuo Chen, Yukun Chen, Yu Zhou, Changyi Wan, et al. 2025. StreamRL: Scalable, Heterogeneous, and Elastic RL for LLMs with Disaggregated Stream Generation. *arXiv preprint arXiv:2504.15930* (2025).
- [21] Yinmin Zhong, Zili Zhang, Bingyang Wu, Shengyu Liu, Yukun Chen, Changyi Wan, Hanpeng Hu, Lei Xia, Ranchen Ming, Yibo Zhu, et al. 2025. Optimizing RLHF training for large language models with stage fusion. In *22nd USENIX Symposium on Networked Systems Design and Implementation (NSDI 25)*. 489–503.